Talanta 286 (2025) 127429

Contents lists available at ScienceDirect

Talanta

journal homepage: www.elsevier.com/locate/talanta

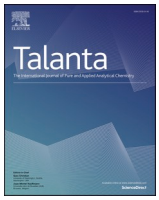

Gold nanoclusters-based dual-mode ratiometric sensing system for selective and sensitive detection of paraquat

Sheng Gong [a], Lingxuan Ma [a], Fan Nie [a], Mai Luo [a], Sijia Wu [a], Ting Wang [a], Yu Yang [b,***], Di Chen [c], Jinchao Wei [a,*], Peng Li [a,**]

[a] Macau Centre for Research and Development in Chinese Medicine, State Key Laboratory of Quality Research in Chinese Medicine, Institute of Chinese Medical Sciences, University of Macau, Macau, 999078, China
[b] Institute of Molecular Medicine and Shanghai Key Laboratory for Nucleic Acid Chemistry and Nanomedicine, Renji Hospital, School of Medicine, Shanghai Jiao Tong University, Shanghai, 200127, China
[c] School of Pharmaceutical Sciences, Zhengzhou University, Zhengzhou, 450001, China

ARTICLE INFO

Keywords:
Pesticide
Fluorescence
Colorimetric
Smartphone
Pollutant detection

ABSTRACT

Unreasonable or illegal utilization of pesticides may lead to pollution of agricultural products, especially with some persistent but effective pesticides. Hence, there is an urgent need to develop sensitive and rapid methods for pesticide detection to ensure the safety of agricultural products. Herein, a dual-mode ratiometric sensing system utilizing two gold nanoclusters (G/R–AuNCs) was designed and constructed for paraquat (PQ) detection, a typical, highly toxic, widely used pesticide. Initially, a ratiometric fluorescent method was developed based on green-emitting (Em~530 nm) and red-emitting (Em~655 nm) gold nanoclusters. Relying on the electrostatic interaction between G-AuNCs and PQ, G-AuNCs were quenched as a sensing unit. R–AuNCs with chemical inertness and excellent stability to PQ served as correction signals. The selective and sensitive detection of PQ was successfully achieved with a satisfactory linear relationship within the range of 5–500 μg/L, and the limit of detection (LOD) was as low as 1.68 μg/L (6.5 nM). Furthermore, PQ can be detected through visual analysis based on smart mobile devices. As the concentration increased, a more noticeable color change occurred, producing a significant shift from yellow to red under 365 nm UV light, resulting in a striking visual effect. This research not only showcases the practical benefits of the dual-mode analytical method but also drives forward the application of ratiometric probes.

1. Introduction

Pesticide residues are an important issue affecting the safety of agricultural products. The irrational or illegal use of pesticides can lead to soil acidification and sclerosis, while pesticide residues in the soil can seep into surface water or groundwater. This ultimately causes a variety of problems, such as contamination of water sources, endangering aquatic organisms, affecting the food chain of water bodies, and jeopardizing ecosystems, and human health [1–4]. Some banned pesticides are still detected in agricultural products due to soil residues or improper use and management [1,5]. Reports indicate that nearly 200, 000 people are poisoned by pesticide-contaminated food each year, accounting for approximately one-third of all food poisoning cases. Pesticides are also responsible for about 60 % of cancer-causing factors. Moreover, nearly 90 % of pesticides make their way into the body through the food chain, atmosphere, and drinking water [6–8].

Paraquat (PQ), a broad-spectrum and highly toxic (toxicological class I), positively charged bipyridilium herbicide ($C_{12}H_{14}N_2)^{2+}$), is currently banned for use in various agricultural processes [9]. PQ poisoning is extremely lethal due to its inherent toxicity, mainly causing multi-organ failure and pulmonary fibrosis, with no effective treatment available [10,11]. PQ residues in agricultural products are strictly regulated in many countries, usually in the range of 40–400 nM [12–14]. Therefore, to develop a convenient, sensitive, and rapid strategy for the

* Corresponding author. Institute of Chinese Medical Sciences, University of Macau, Avenida da Universidade Taipa, Macau, China.
** Corresponding author. Institute of Chinese Medical Sciences, University of Macau, Avenida da Universidade Taipa, Macau, China.
*** Corresponding author. Institute of Molecular Medicine and Shanghai Key Laboratory for Nucleic Acid Chemistry and Nanomedicine, Renji Hospital, School of Medicine, Shanghai Jiao Tong University, Shanghai, 200127, China.
E-mail addresses: yuyang@shsmu.edu.cn (Y. Yang), wjc551@hotmail.com, jinchaowei@um.edu.mo (J. Wei), pli1978@hotmail.com, pengli@um.edu.mo (P. Li).

https://doi.org/10.1016/j.talanta.2024.127429
Received 21 September 2024; Received in revised form 9 December 2024; Accepted 18 December 2024
Available online 19 December 2024

detection of PQ in agricultural products is essential. Various methods including high-performance liquid chromatography [15,16], colorimetric analysis [17,18], surface-enhanced Raman spectroscopy [19–21], electrochemical analysis [14,22], host-guest recognition-based fluorescence analysis [23,24], chemiluminescence [25,26], and aptasensors [27,28], have been established for PQ detection. Among them, fluorescence analysis is highly sensitive and selective, capable of detecting targets at extremely low concentrations [29,30]. The dual nature of the cationic and conjugated π-systems of PQ makes it a good electron acceptor or a potential anionic dye quencher [31]. The high applicability of PQ detection using a quenching-based method with a synthetic anionic fluorescent probe has been demonstrated [32]. The integration of fluorescence and other techniques, known as the dual-mode method, provides substantial benefits in accurately assessing trace targets both quantitatively and qualitatively [33–35]. Currently, there is a scarcity of dual-mode ratiometric methods for detecting PQ.

In this study, a ratiometric fluorescent probe with green- and red-emitting gold nanoclusters (G/R–AuNCs) was designed for PQ detection at first (Scheme 1). The dual-emitting ratiometric sensing system was constructed by direct mixing without chemical coupling, which has built-in corrections to eliminate unavoidable environmental interferences. As a response signal, G-AuNCs showed sensitive green fluorescence quenching due to electrostatic attraction, while R–AuNCs act as a reference signal. Drawing on the noticeable color disparities between two probes visible to the naked eye under UV light, we then formulated a visual analytical method. With the integration of the fluorescence and visualization, this dual-mode ratiometric sensing system was successfully applied for detecting PQ residues in several real plant samples.

2. Experiments

2.1. Chemicals

Hydrogen tetrachloroaurate (III) trihydrate ($HAuCl_4 \cdot 3H_2O$, ≥99.9 %), bovine serum albumin (BSA, ≥98.0 %) and L-arginine were obtained from Shanghai Aladdin Biochemical Technology Co., Ltd. 6-aza-2-thiothymine (ATT), tetramethylammonium bromide, 1-hexadec ylpyridin-1-ium chloride, β-diphosphopyridine nucleotide, and choline chloride were obtained from Shanghai Titan Scientific Co., Ltd. Paraquat dichloride, carbendazim, dimethoate, parathion methyl, chlorpyifos, diquat dibromide were supplied by Dr. Ehrenstorfer GmbH (Germany). All reagents were used directly without further purification unless otherwise stated.

2.2. Instruments

Transmission electron microscopy (TEM) images were obtained using Talos F200S transmission electron microscopy (Thermo Fisher Scientific, USA) at an acceleration of 200 kV to obtain size and morphological characteristics. The UV–Vis absorption and fluorescence spectra were collected by a DR 6000 UV–Vis spectrophotometer (HACH, USA) and a FluoroMax-4 fluorescence spectrometer (HORIBA Scientific, USA), respectively. The fluorescent lifetime data were collected with a FLS980 Combined Time Resolved & Steady State Photoluminescence Spectrometer (Edinburgh Instruments, UK). Zeta potential analysis was performed by a Zetasizer Nano ZSP (Malvern Panalytical, UK). ZF-8N UV-viewing cabinet was also used in the visual analysis section (Shanghai Jiapeng, China). The ultrapure water utilized was sourced from a Milli-Q water purification system (Merck Millipore, USA).

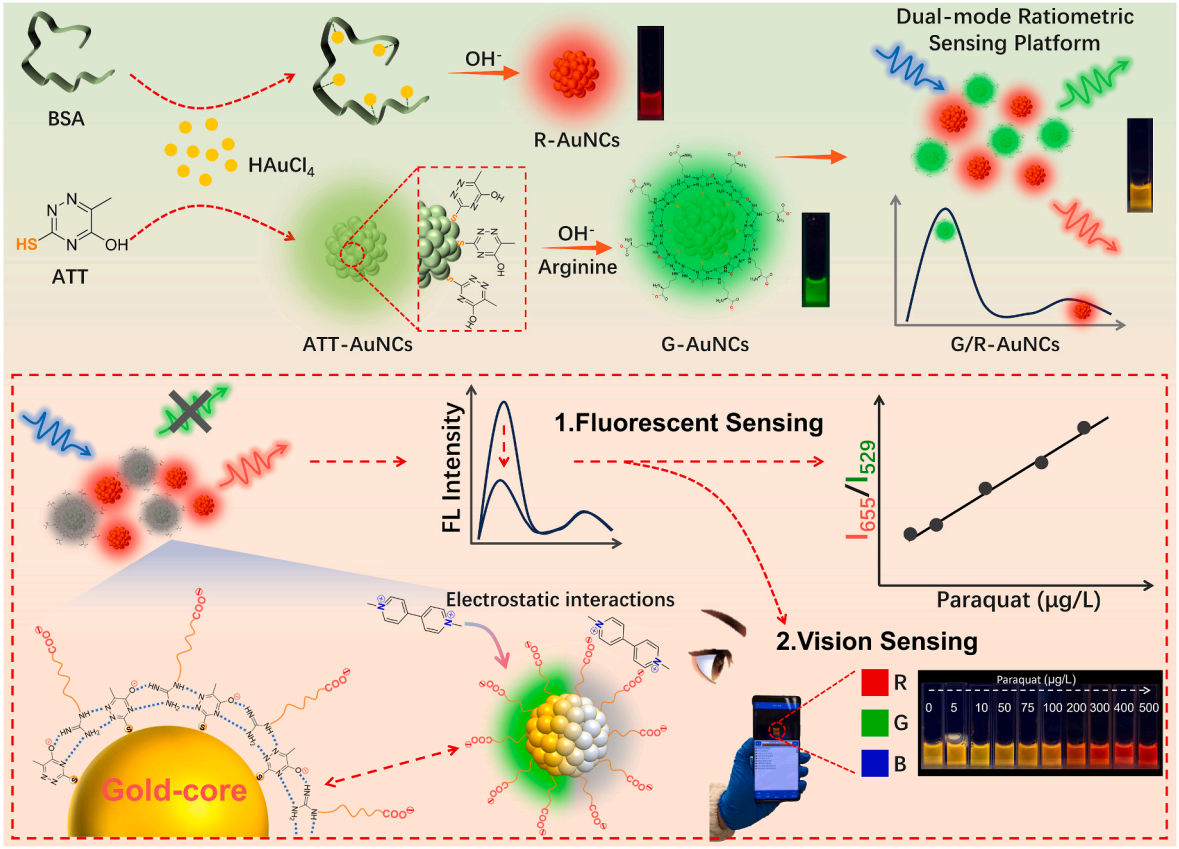

Scheme 1. Schematic of the gold nanoclusters-based dual-mode ratiometric sensing system for selective and sensitive detection of PQ.

2.3. Preparation of G-AuNCs and R–AuNCs

All glassware needs to be processed with *Aqua Regia* for at least 24 h before use. G-AuNCs were synthesized based on steps from previous reported studies with slight modifications [36,37]. Briefly, 5 mL 80 mM ATT containing 200 mM NaOH was added to a 5 mL 29.5 mM $HAuCl_4$ solution (10 mg/mL). The mixed solution was stirred continuously for 1 h at room temperature in the dark. The ATT-AuNCs were obtained by ultrafiltration, and the volume was reconstituted to 10 mL. The ATT-AuNCs were carefully stored at 4 °C in a dark environment to ensure their quality and effectiveness when used. Add 2 mL of 40 mM L-arginine to 18 mL of the prepared ATT-AuNC solution and let the mixture react at 37 °C for 24 h. The G-AuNCs were purified using ultrafiltration and then reconstituted to a volume of 20 mL. Then, they can be stored at 4 °C in a dark environment for up to 6 months.

R–AuNCs were synthesized using previous studies reported with simple adjustments [38,39]. The solution was preheated to 37 °C. Then, 5 mL of 10 mM $HAuCl_4$ solution was added to 5 mL of 50 mg/mL BSA solution, and vigorously stirred for 5 min. A 0.5 mL NaOH solution with a concentration of 1 M was added to the mixture. The reaction was then allowed to proceed for 12 h at 37 °C while being vigorously stirred. The synthesized R–AuNCs were obtained by ultrafiltration and then reconstituted to 10 mL.

2.4. Fluorescence detection for PQ

For the fluorescence detection of PQ, 1.0 μL of G-AuNCs and 50.0 μL of R–AuNCs were dispersed in 99.0 μL of ultrapure water to obtain the G/R–AuNCs probe solution. Following this, 50.0 μL of PQ standard solution (0, 2.5, 5, 10, 50, 75, 100, 200, 300, 400 and 500 μg/L) was introduced, and the mixture was carefully blended. Photoluminescence spectra of G/R–AuNCs were recorded to examined the analytical performance. The calibration curve was plotted between the fluorescence intensity ratio (I_{655}/I_{529}) and the PQ concentration. The sensing system's selectivity was assessed by testing it with various interferents, including K^+, Na^+, Mg^{2+}, Ca^{2+}, Ba^{2+}, Ni^{2+}, Fe^{3+}, NH_4^+, tetramethylammonium bromide, 1-hexadec ylpyridin-1-ium chloride, β-diphosphopyridine nucleotide, choline chloride, diquat dibromide, methyl paraoxon, naled, dichlorvos, dimethoate, parathion methyl, chlorpyifos, and carbendazim. The excitation wavelength of the PQ probe was set at 470 nm, and the fluorescence emission intensity was collected in the range of 485~720 nm.

2.5. Procedure of visual detection

The visual inspection process was identical to the fluorescence inspection process described above, except that the various solutions were added in 5-fold amounts to bring their total volume to 1000 μL. Sample images were captured by a VIVO X90Pro+ smartphone (the ISO value was 400, f/1.75, and the shutter speed was 0.3 s). The photos were taken under a 365 nm UV lamp inside a dark box. Relying on the smartphone APP (Color Recognizer V8.101, Xiamen Xiyi Technology Co., Ltd.), the intensities on the red channel to green channel ratio (R/G) of the sample at 365 nm were read to calculate the calibration curve.

2.6. Real sample analysis

Two plant samples (Notoginseng Radix et Rhizoma and Ginseng Radix et Rhizoma) were selected to verify the feasibility of this method, which were supplied by a pharmacy in Guangzhou, China. Preprocessing procedures for samples were developed based on previous work [28,40]. The sample was chopped into small uniform pieces. 2 g of the sample was extracted with 10 mL of 25 % ethanol solution in a 15 mL centrifuge tube followed by sonication for 10 min at room temperature. The solution was centrifuged at 3500×*g* for 10 min to ensure complete removal of insoluble materials. Subsequently, 8 mL of the supernatant was taken, evaporated to dryness, and redissolved in 1 mL of 25 % ethanol solution for analysis. 500 mL of water samples were taken from campus lakes and laboratory faucets, respectively, and the samples were filtered through a 0.22 μm microporous filter membrane to remove solid impurities. We spiked known concentrations of PQ into samples following the aforementioned procedures to conduct a recovery study.

3. Results and discussions

3.1. Characterization of G-AuNCs and R–AuNCs

As provided in Scheme 1, AuNCs with intense green and red emission were prepared using ATT/Arginine and BSA. The preparation methods for R–AuNCs are well established, and the ratio of ATT to arginine was optimized to make it suitable for PQ sensing. As the ratio of added arginine increased, the fluorescence intensity of ATT-AuNCs was significantly enhanced (Fig. S1A–C). Subsequently, employing a target concentration of 10 μg/L PQ, the findings demonstrated that an ATT to Arg ratio of 9:1 in the probe yielded the most effective detection results, accompanied by the lowest standard deviation (Fig. S1D). Finally, the 9:1 ratio was selected as the optimal preparation method for G-AuNCs.

To investigate the optical performance of AuNCs, fluorescent and UV–Vis absorption spectra were obtained, and the results are shown in Fig. 1. The aqueous solutions of G-AuNCs and R–AuNCs were observed to be light yellow (Fig. 1A) and brown (Fig. 1D), respectively. They emitted strong green (Fig. 1G) and red (Fig. 1H) fluorescence under 365 nm UV lamp (Fig. S2), which proved that the two prepared AuNCs had excellent fluorescence behavior, as confirmed by the fluorescence lifetime decay curves (Fig. 1I). The prepared G-AuNCs and R–AuNCs both showed the expected strong fluorescence with maximum emission wavelengths of ~530 nm and ~655 nm, respectively. TEM images showed that the sizes of G-AuNCs and R–AuNCs were 1~3 nm (Fig. 1C and F), respectively. The lattice spacing of both AuNCs is ~0.2 nm, which corresponds to the crystal plane of gold [41]. In addition, the results of zeta potential analysis of G/R–AuNCs (Fig. S3) also indicate that G-AuNCs and R–AuNCs synergistically keep the performance of PQ probes.

3.2. Constructing the G/R–AuNCs sensing system

In the sensing strategy for detecting PQ in this study, a mixture of two AuNCs (G- and R-) in specific ratios enables the realization of fluorescent detection of PQ in water, which works as shown in Scheme 1. The presence of abundant carboxyl groups on the surface of G-AuNCs makes it highly susceptible to electrostatic interactions with PQ, which is quenched as a PQ response signal. R–AuNCs were used as correction signals due to their chemical inertness to PQ, while the green fluorescence of G-AuNCs was significantly reduced in the presence of PQ (Fig. 2A and B). These remarkable features allow us to fabricate PQ sensing platforms by simply mixing two AuNCs.

Typically, ratiometric fluorescent probes produce stronger visually perceived color changes than single-emission probes [42,43]. This study employs a dual-mode sensing strategy, combining fluorescence and visual detection, for the sensing of PQ. From the perspective of fluorescence, the concentration/volume of R–AuNCs has a slight effect on the detection of PQ, as it serves as an auxiliary internal reference signal. For visual detection, the ratio of the two AuNCs is more important, as it needs to ensure that the probe shows a clear color change in response to PQ concentration under 365 nm UV light. To maximize the visual sensing performance of the dual-emission sensing platform, the ratio of G-AuNCs to R–AuNCs was optimized. Based on the reaction of G/R AuNCs to the PQ as shown in Fig. S4, a ratio of 1:50 was selected to guarantee a noticeable color change from yellow to red, which improves the visual detection of PQ. The 3D excitation-emission maps of G-AuNCs (Fig. 2C and Fig. S5A) and R–AuNCs (Fig. 2C and Fig. S5B) were collected, and the maximum emission wavelengths of the two AuNCs did

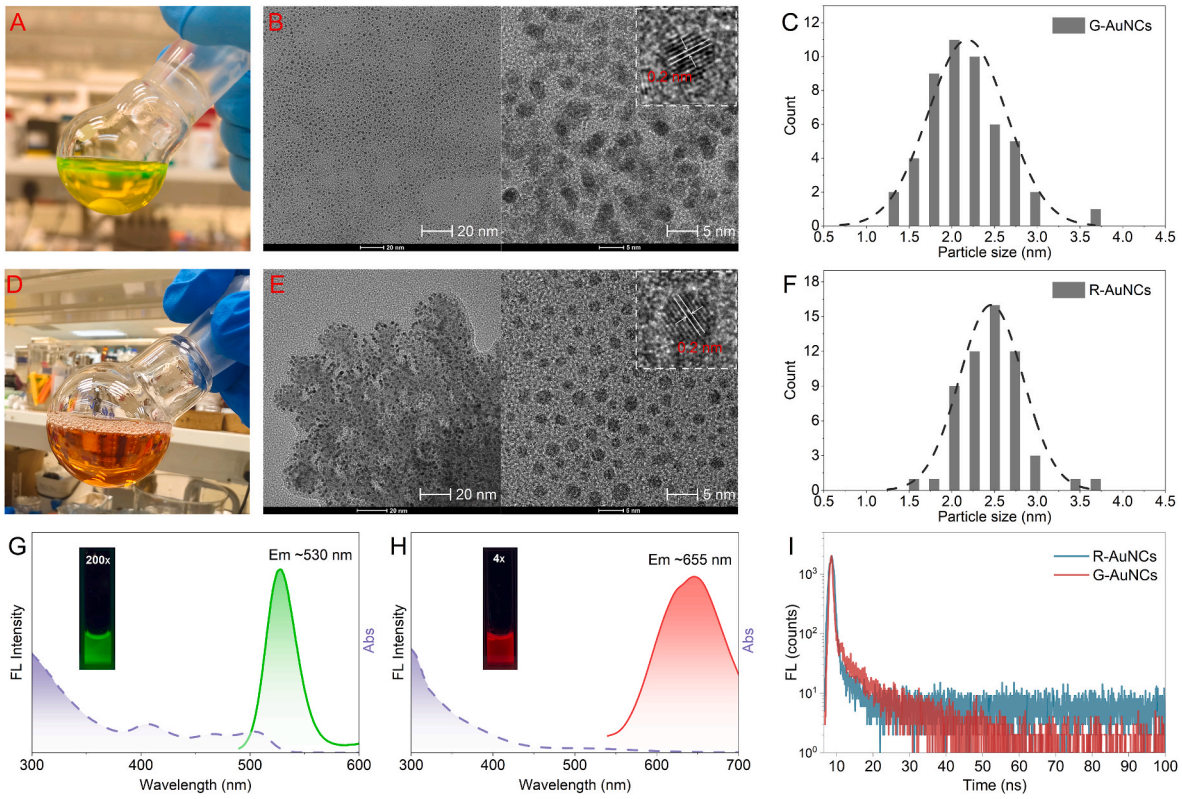

Fig. 1. Optical and morphological characterizations of AuNCs. Photographs of G-AuNCs (A) and R–AuNCs (D). TEM image and corresponding lateral size distribution of G-AuNCs (B–C) and R–AuNCs (E–F). UV–vis absorption spectra (purple line), and emission spectra (green line and red line) of G-AuNCs (G) and R–AuNCs (H). Insets are photos of the two AuNCs solution under a UV lamp (365 nm). Time-resolved fluorescence spectra of AuNCs (I). (For interpretation of the references to color in this figure legend, the reader is referred to the Web version of this article.)

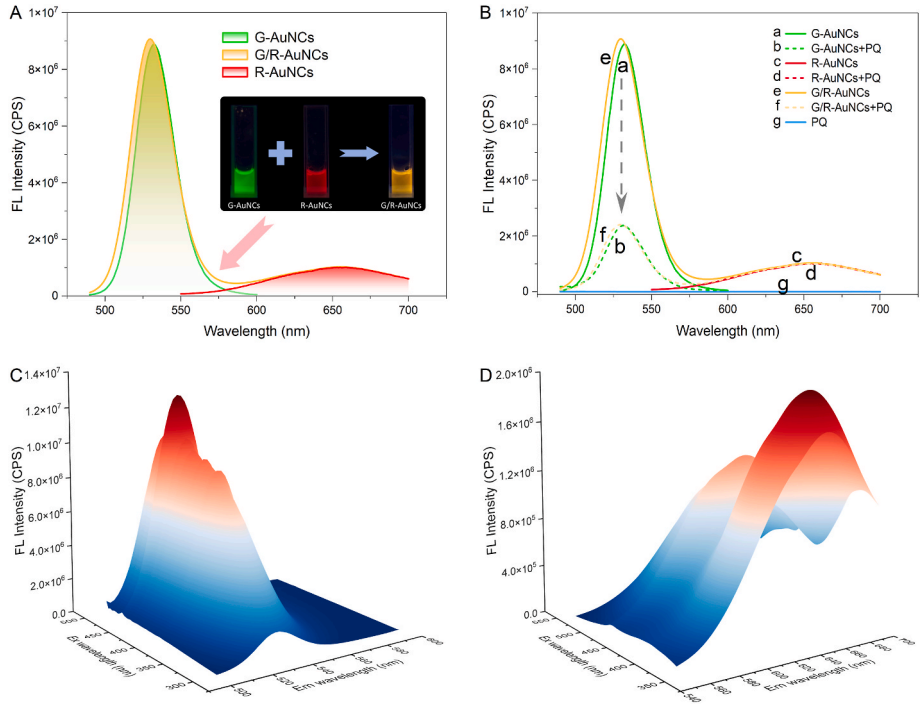

Fig. 2. The fluorescence spectra of G-AuNCs, R–AuNCs, and G/R–AuNCs (A). Fluorescence spectra under different conditions (B): (a) G-AuNCs, (b) G-AuNCs + PQ, (c) R–AuNCs, (d) R–AuNCs + PQ, (e) G/R–AuNCs, (f) G/R–AuNCs + PQ, and (g) PQ. The 3D excitation/emission spectra of G-AuNCs (C) and R–AuNCs (D).

not change with the shift of the excitation wavelengths, so 470 nm was chosen as the excitation wavelength of the G/R–AuNCs for the subsequent experiments.

G/R–AuNCs present favorable stability, which is important for establishing a reliable sensing platform. Both G-AuNCs and R–AuNCs are dissolved and stabilized in water, while PQ is a bipyridinium cationic salt ($(C_{12}H_{14}N_2)^{2+}$). Therefore, the detection of PQ will be faster and more sensitive in a solution with higher water content. As a result, it is adequate to use only water as the detection system. G/R–AuNCs responded rapidly to PQ, with a rapid decrease in fluorescence intensity within 30 s, followed by stabilization (Fig. S6).

3.3. Mechanisms of PQ sensing

Interactions between PQ and the probes were studied using a combination of zeta potential analysis, UV–Vis spectroscopy, and fluorescence spectroscopy. Additionally, these techniques were employed to explore the potential sensing mechanisms involved. The addition of PQ had no significant effect on the fluorescence intensity of R–AuNC, indicating that it is not related to R–AuNC (Fig. 2B). And the introduction of PQ did not result in the aggregation of G-AuNCs. The average potential value of G/R–AuNCs increased from −45.6 mV to −42.47 mV when PQ was added (Fig. S7). Fluorescence quenching of G-AuNCs may be mediated by electrostatic interactions. PQ belongs to a bipyridinium cationic salt [44]. Several recent studies have reportedly utilized negatively charged molecules to monitor paraquat [9,31,32]. In this study, G/R–AuNCs were also negatively charged (Fig. S7). Time-resolved fluorescence lifetime data further confirmed this static quenching mechanism (Fig. S8), which indicates that no FRET process is involved [45,46].

The possible involvement of PET has also been explored, taking into account the unique structure of PQ. Amino groups play a vital role by donating electrons to electron-deficient molecules, resulting in the creation of stable Meissenheimer complexes [43,47,48]. The primary amino group in arginine acts as an electron donor in the presence of PQ, which acts as a strong electron acceptor. As shown in Fig. S9, adding PQ did not cause any new absorption peaks to appear, indicating that no new complexes were formed in the detection system. This suggests that PET effects are not involved in the process either.

3.4. Fluorescent and ratiometric sensing of PQ based on dual-emitting sensing system

Fluorescence intensity measurements were collected after the addition of different concentrations of PQ to verify the utility of this ratiometric sensing system. As the concentration of PQ is raised from 2.5 μg/L to 500 μg/L, the fluorescence intensity of the G/R–AuNCs (529 nm) gradually decreased, while the emission at 655 nm basically remained stable (Fig. 3A and B). Thus, a ratiometric method was developed for detecting PQ with good linear correlation in the concentration range of 5–500 μg/L. The calibration curve equation was $y = 4.31\times10^{-4}x + 0.0805$ with a correlation coefficient of 0.9968 and adjusted R-squared (R^2_{adj}) of 0.9928 (Fig. 3C). The LOD for PQ was calculated to be 1.68 μg/L (6.5 nM) by using the 3σ rule [49], which was much lower than the residue limits of PQ (<0.2 mg/kg) in agricultural products stipulated by the *National Food Safety Standard* - Maximum residue limits for pesticides in food. Notably, this work demonstrates superior performance compared to most previous methods, while also reducing the analysis time (Table S1). This analytical strategy also achieves satisfactory results (PQ: 5–500 μg/L) using other work platforms (Fig. S10).

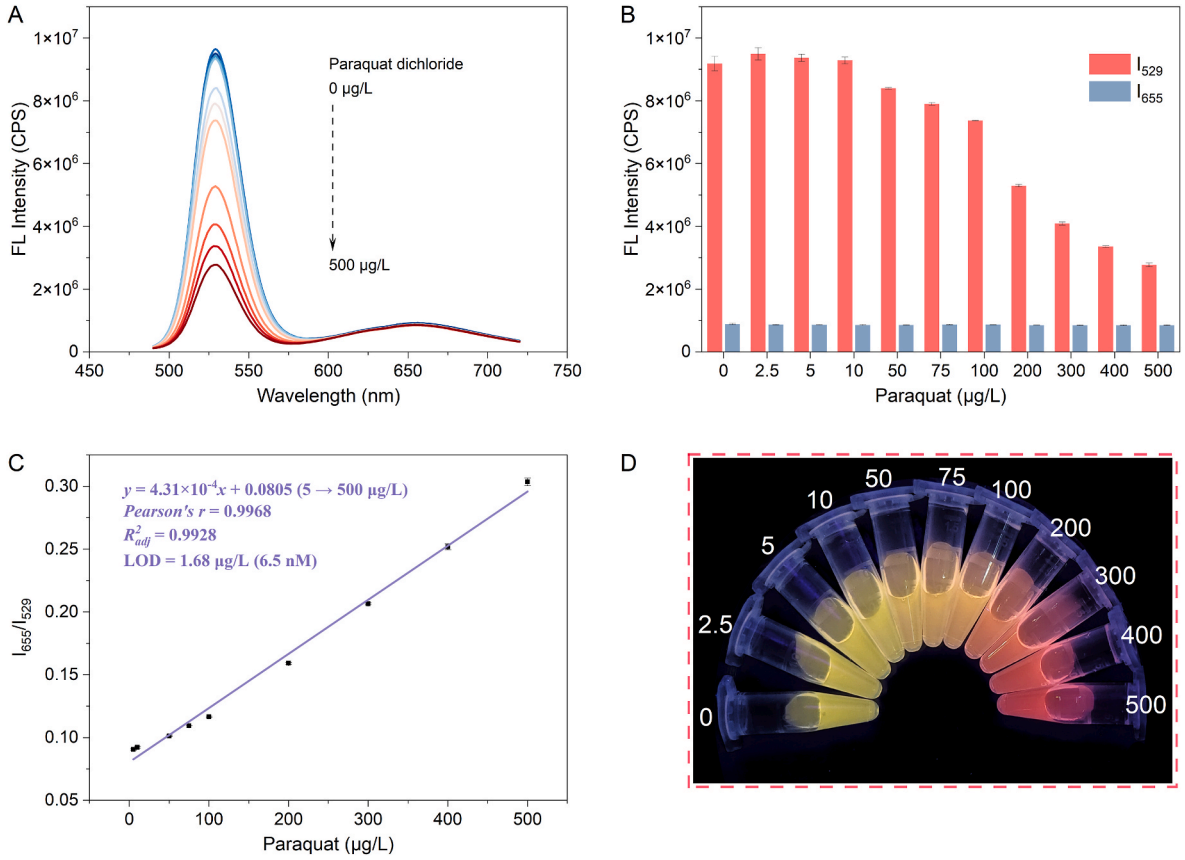

Fig. 3. (A) Fluorescence spectra of the dual-emitting ratiometric probe with PQ added (0 → 500 μg/L) and its fluorescence intensity (B) at 529 nm and 655 nm, respectively. (C) Linear calibration curve of fluorescence intensity ratio (I_{655}/I_{529}) with added PQ concentration (5, 10, 50, 75, 100, 200, 300, 400 and 500 μg/L). (D) Picture of G/R–AuNCs probe under 365 nm UV lamp after adding PQ.

Meanwhile, the G/R–AuNCs probes exhibit a ratiometric fluorescence response to PQ, leading to a noticeable shift in emission color from yellow to red, readily observable to the naked eye under 365 nm UV lamp (Fig. 3D). This unique characteristic enables practical on-site detection of PQ using the present G/R–AuNCs probes.

3.5. Visual and ratiometric sensing of PQ

We collected the color changes resulting from the interaction of PQ with the probe under UV light using a smartphone (Fig. 4A). With increasing PQ concentration, the color change became more obvious thus creating a vision shock. As the concentration increased (10 → 500 μg/L), the probe produced a significant change from yellow to red under 365 nm excitation (Fig. 4B). In addition, based on the analysis of the red channel/green channel ratio (R/G) extracted from the RGB results (Fig. 4C), a linear relationship was obtained for PQ in the concentration range of 10–500 μg/L with a correlation coefficient of 0.9941 and adjusted R-squared (R^2_{adj}) of 0.9863. In conclusion, the proposed smartphone-assisted colorimetric method also showed satisfactory performance in the colorimetric analysis of PQ.

3.6. Selectivity

The selectivity was investigated by collecting the fluorescence spectra of various interferents, including multiple quaternary ammonium salts, pesticides, and ions, in response to G/R–AuNCs (Fig. S11). We first investigated the effect of high concentrations (500 μg/L) of quaternary ammonium salts on the dual-mode probe. The results showed that other quaternary ammonium salts did not affect the performance of the probe (Fig. S12). Interestingly, both diquat and paraquat (PQ) have a bipyridine structure, but the probe's response to PQ was much higher than to diquat. Employing the Coulombic force between positive and negative charges to design fluorescent probes is a promising strategy. By carefully designing the ligands or functional groups on the surface of the gold core, it is possible to achieve sensing for specific targets [50–52]. The detection performance of G/R–AuNCs for pesticides is shown in Fig. 5A. The presence of other pesticides resulted in weaker fluorescence changes, suggesting that G-AuNCs has a specific recognition ability for PQ. Similarly, the effects from the added ion interferences were negligible except PQ itself (Fig. 5B). These results suggest that the G/R–AuNCs probe system can achieve selective ratiometric sensing of PQ, providing a promising monitoring strategy for assessing the safety and quality of paraquat-contaminated agricultural products.

3.7. Practicability

We spiked PQ into two samples of economically important agricultural products (e.g., Notoginseng Radix et Rhizoma and Ginseng Radix et Rhizoma) and analyzed the recovery rates. Local lake water and tap water samples were also detected. The results are shown in Fig. 6. The recoveries of the actual samples analyzed based on fluorescence spectra were 90 %–110 %, which were in line with the requirements of the *Chinese Pharmacopoeia* (2020) for the detection of pesticide residues (70 %–120 %), demonstrating that the ratiometric fluorescent probe can reliably and effectively detect PQ in practical situations. Visual analytics likewise presents notable application potential.

4. Conclusions

In this work, we have utilized two gold-nanocluster probes for the dual-mode ratiometric sensing of paraquat. By utilizing R–AuNCs as the

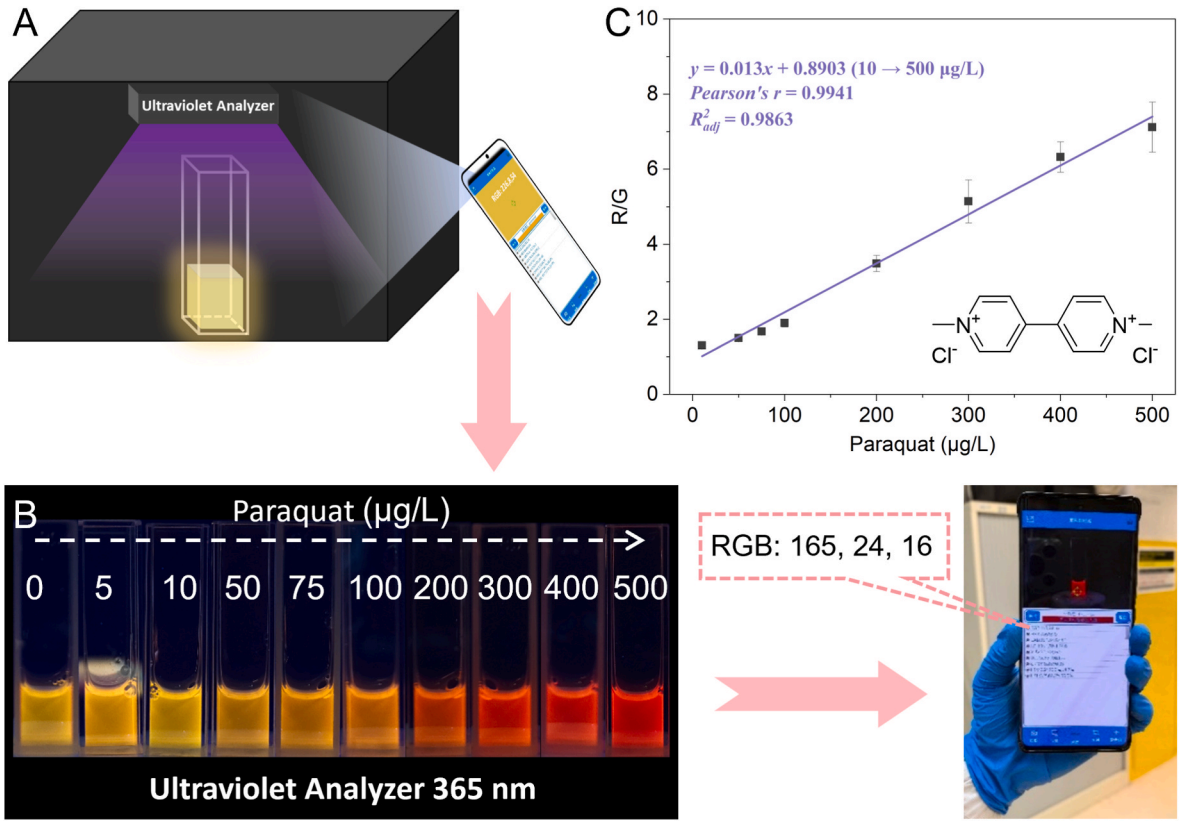

Fig. 4. A smartphone recognizes the RGB values of probe (A). Color change of the probe when different concentrations of PQ were added under 365 nm UV lamp (B). Relationship between probe R/G values and PQ concentration (C). (For interpretation of the references to color in this figure legend, the reader is referred to the Web version of this article.)

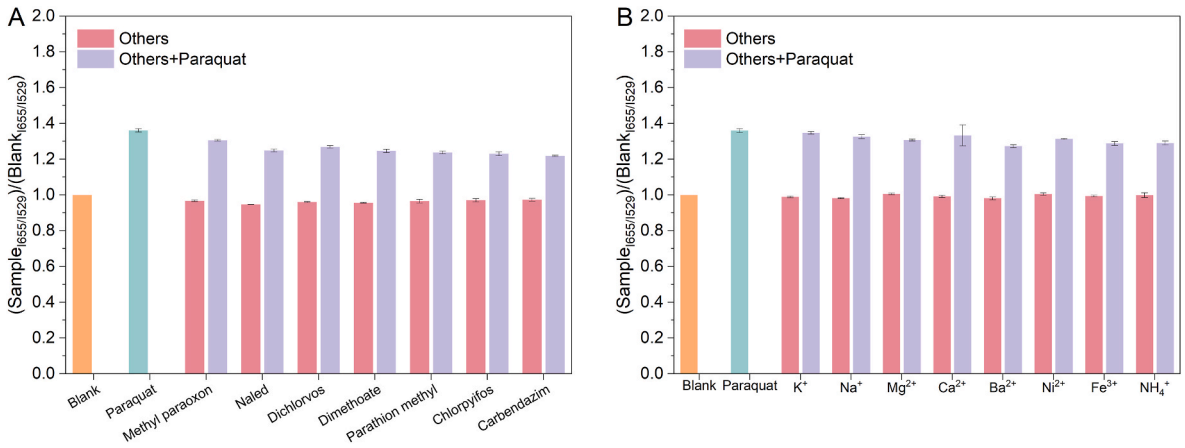

Fig. 5. The response of G/R–AuNCs to multiple pesticides (A), and ions (B) were evaluated. The concentrations of the interfering substances were 100 μg/L for pesticides, and 2 μM for ions, respectively. The ion concentration was ~5 times higher than that of the pesticides.

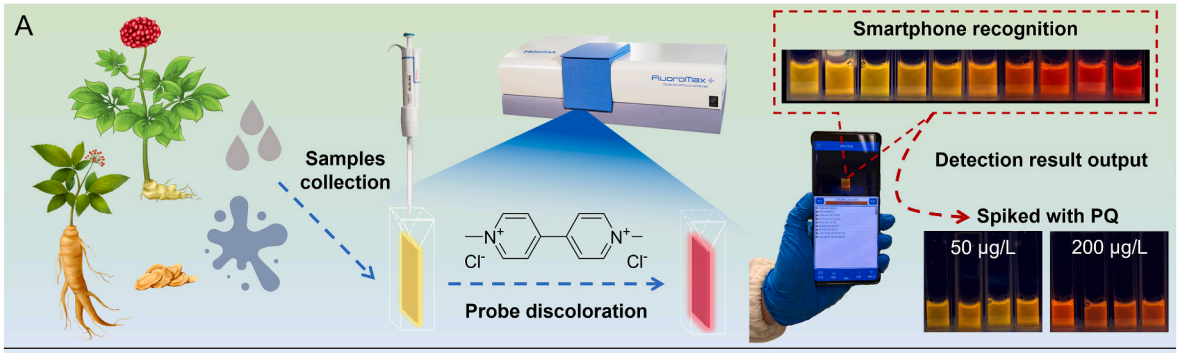

B

Sample	Fluorescence detection of PQ				C Visual detection of PQ			
	Spiked (μg/L)	Found	Recovery (n=3, %)	RSD (n=3, %)	Spiked (μg/L)	Found	Recovery (n=3, %)	RSD (n=3, %)
Notoginseng Radix et Rhizoma	50	48.64	97.28	4.43	50	42.86	85.72	5.68
	200	192.32	96.16	1.29	200	186.52	93.26	4.14
Ginseng Radix et Rhizoma	50	53.34	106.68	4.84	50	48.66	97.33	5.98
	200	217.17	108.59	3.80	200	204.37	102.19	5.25
Lake water	50	49.18	98.36	3.59	50	47.05	94.1	4.53
	200	209.98	104.99	2.02	200	193.31	96.65	2.55
Tap water	50	50.20	100.4	4.26	50	51.72	103.44	4.66
	200	203.48	101.74	3.89	200	202.51	101.26	2.61

Fig. 6. (A) Schematic of the fluorescence/visual sensing platform for PQ detection in real samples. The spiked recovery tests for PQ in real samples were based on fluorescence sensing (B) and visual analysis (C).

internal standard, the fabricated sensor demonstrates swift response time, broad linear range, and exceptional selectivity. Based on various characterizations, static quenching is unequivocally revealed as the intrinsic mechanism for the fluorescence analysis of PQ. Through innovative design and careful optimization, the system effectively produced a distinct color change from yellow to red. Subsequently, a smartphone-assisted ratiometric method was successfully explored for detecting PQ, showcasing excellent visualization capabilities. To sum up, this research showcases the efficacy of the dual-mode method as an innovative approach for conducting on-site analysis. It also highlights the significant potential for the practical implementation of smart device-assisted platforms.

CRediT authorship contribution statement

Sheng Gong: Writing – original draft, Methodology, Investigation. **Lingxuan Ma:** Validation, Data curation. **Fan Nie:** Investigation, Data curation. **Mai Luo:** Methodology. **Sijia Wu:** Methodology. **Ting Wang:** Investigation, Data curation. **Yu Yang:** Resources, Formal analysis. **Di Chen:** Resources. **Jinchao Wei:** Writing – review & editing, Supervision, Project administration, Funding acquisition, Conceptualization. **Peng Li:** Supervision, Project administration, Funding acquisition.

Declaration of competing interest

The authors declare that they have no known competing financial interests or personal relationships that could have appeared to influence

the work reported in this paper.

Acknowledgments

We gratefully acknowledge the financial support from Macau Science and Technology Development Fund (0014/2022/ITP, 0031/2022/AGJ, and 005/2023/SKL), Guangdong Basic and Applied Basic Research Foundation (2024A1515030214)), and the Research Committee of the University of Macau (SRG2022-00035-ICMS, MYRG-2022-00226-ICMS, MYRG-CRG2022-00016-ICMS, MYRG-GRG2023-00205-ICMS and MYRG-GRG2023-00234-ICMS-UMDF).

Appendix A. Supplementary data

Supplementary data to this article can be found online at https://doi.org/10.1016/j.talanta.2024.127429.

Data availability

Data will be made available on request.

References

[1] M.S. Goh, S.D. Lam, Y. Yang, M. Naqiuddin, S.N.K. Addis, W.T.L. Yong, V. Luang-In, C. Sonne, N.L. Ma, Omics technologies used in pesticide residue detection and mitigation in crop, J. Hazard Mater. 420 (2021) 126624.
[2] S. Sindhu, A. Manickavasagan, Nondestructive testing methods for pesticide residue in food commodities: a review, Compr. Rev. Food Sci. Food Saf. 22 (2) (2023) 1226–1256.
[3] M. Zhao, J. Wu, D.M. Figueiredo, Y. Zhang, Z. Zou, Y. Cao, J. Li, X. Chen, S. Shi, Z. Wei, J. Li, H. Zhang, E. Zhao, V. Geissen, C.J. Ritsema, X. Liu, J. Han, K. Wang, Spatial-temporal distribution and potential risk of pesticides in ambient air in the North China Plain, Environ. Int. 182 (2023) 108342.
[4] I. Md Meftaul, K. Venkateswarlu, R. Dharmarajan, P. Annamalai, M. Megharaj, Pesticides in the urban environment: a potential threat that knocks at the door, Sci. Total Environ. 711 (2020) 134612.
[5] L. Chen, Z. Cheng, M. Luo, T. Wang, L. Zhang, J. Wei, Y. Wang, P. Li, Fluorescent noble metal nanoclusters for contaminants analysis in food matrix, Crit. Rev. Food Sci. Nutr. 63 (19) (2023) 3519–3537.
[6] X.Q. Sun, F. An, Q. Lu, C.Y. Li, J.Y. Luo, M.H. Yang, Residual status, toxicity, and analytical method of banned pesticides in traditional Chinese medicines, China J. Chin. Mater. Med. 47 (3) (2022) 611–627.
[7] K.C. Wu, Y.Y. Chen, Regulatory control of highly hazardous pesticides to prevent self-poisoning, Lancet Global Health 5 (10) (2017) e959–e960.
[8] R. Kaur, D. Choudhary, S. Bali, S.S. Bandral, V. Singh, M.A. Ahmad, N. Rani, T. G. Singh, B. Chandrasekaran, Pesticides: an alarming detrimental to health and environment, Sci. Total Environ. 915 (2024) 170113.
[9] Z. Zhao, F. Zhang, Z. Zhang, A facile fluorescent "turn-off" method for sensing paraquat based on pyranine-paraquat interaction, Spectrochim. Acta Mol. Biomol. Spectrosc. 199 (2018) 96–101.
[10] N. Rashidipour, S. Karami-Mohajeri, A. Mandegary, R. Mohammadinejad, A. Wong, M. Mohit, J. Salehi, M. Ashrafizadeh, A. Najafi, A. Abiri, Where ferroptosis inhibitors and paraquat detoxification mechanisms intersect, exploring possible treatment strategies, Toxicology 433–434 (2020) 152407.
[11] L. Hu, Q. Lan, C. Tang, J. Yang, X. Zhu, F. Lin, Z. Yu, X. Wang, C. Wen, X. Zhang, Z. Lu, Abnormalities of serum lipid metabolism in patients with acute paraquat poisoning caused by ferroptosis, Ecotoxicol. Environ. Saf. 266 (2023) 115543.
[12] D. Li, Q. Zheng, Z. Li, Y. Xie, L. Zhang, L. Zhao, Y. Yang, J. Liu, R. Na, Research progress of pyridine pesticides, Agrochemicals 61 (10) (2022) 705–712.
[13] T. Nasir, G. Herzog, M. Hebrant, C. Despas, L. Liu, A. Walcarius, Mesoporous silica thin films for improved electrochemical detection of paraquat, ACS Sens. 3 (2) (2018) 484–493.
[14] C. Yuan, C. Tang, X. Zhan, M. Zhou, L. Zhang, W.T. Chen, A. Abdukayum, G. Hu, ZIF-67 based CoS(2) self-assembled on graphitic carbon nitride microtubular for sensitive electrochemical detection of paraquat in fruits, J. Hazard Mater. 467 (2024) 133715.
[15] C. Hao, X. Zhao, D. Morse, P. Yang, V. Taguchi, F. Morra, Optimized liquid chromatography tandem mass spectrometry approach for the determination of diquat and paraquat herbicides, J. Chromatogr. A 1304 (2013) 169–176.
[16] Z. Mao, Y. Yu, H. Sun, W. Xie, H. Zhao, Q. Jiang, Y. Sun, Y. Cao, F. Chen, Development and validation of a sensitive and high throughput UPLC-MS/MS method for determination of paraquat and diquat in human plasma and urine: application to poisoning cases at emergency departments of hospitals, Forensic Toxicol. 40 (1) (2022) 102–110.
[17] W. Siangproh, T. Somboonsuk, O. Chailapakul, K. Songsrirote, Novel colorimetric assay for paraquat detection on-silica bead using negatively charged silver nanoparticles, Talanta 174 (2017) 448–453.
[18] S. Seetasang, T. Kaneta, Portable two-color photometer based on paired light emitter detector diodes and its application to the determination of paraquat and diquat, Microchem. J. 171 (2021) 106777.
[19] M.H. Lin, L. Sun, F.B. Kong, M.S. Lin, Rapid detection of paraquat residues in green tea using surface-enhanced Raman spectroscopy (SERS) coupled with gold nanostars, Food Control 130 (2021) 108280.
[20] N.L. Li, M.P. Zhang, X. Geng, R.R. Liu, X. Meng, W. Zou, W.W. Chen, H. Shao, C. J. Wang, Rapid and highly sensitive determination of unexpected diquat and paraquat in biological fluids by electro-enhanced SPME-SERS, Sensor Actuat B-Chem 382 (2023) 133504.
[21] N. Kamkrua, T. Ngernsutivorakul, S. Limwichean, P. Eiamchai, C. Chananonnawathorn, V. Pattanasetthakul, R. Ricco, K. Choowongkomon, M. Horprathum, N. Nuntawong, T. Bora, R. Botta, Au nanoparticle-based surface-enhanced Raman spectroscopy aptasensors for paraquat herbicide detection, ACS Appl. Nano Mater. 6 (2) (2023) 1072–1082.
[22] H. El Harmoudi, M. Achak, A. Farahi, S. Lahrich, L. El Gaini, M. Abdennouri, A. Bouzidi, M. Bakasse, M.A. El Mhammedi, Sensitive determination of paraquat by square wave anodic stripping voltammetry with chitin modified carbon paste electrode, Talanta 115 (2013) 172–177.
[23] E. Sanabria Espanol, M. Maldonado, Host-guest recognition of pesticides by calixarenes, Crit. Rev. Anal. Chem. 49 (5) (2019) 383–394.
[24] K. Kanagaraj, M. Alagesan, Y. Inoue, C. Yang, Solvation effects in supramolecular chemistry, in: J.L. Atwood (Ed.), Comprehensive Supramolecular Chemistry II, Elsevier, Oxford, 2017, pp. 11–60.
[25] N. Kishikawa, S. Higuchi, K. Ohyama, K. Nakashima, N. Kuroda, A simple and rapid chemiluminescence assay for on-site analysis of paraquat using a portable luminometer, Forensic Toxicol. 31 (2) (2013) 301–306.
[26] F. Liu, H. Shi, X. Xu, W. Kang, Z. Li, Flow injection chemiluminescence determination of paraquat using luminol and Ag(III) complex, Asian J. Chem. 23 (2) (2010) 795–798.
[27] Y.Y. Liu, B.Y. Liu, L. Xia, H.Y. Yu, Q.D. Wang, Y.E. Wu, Cationic polyelectrolyte as powerful capture molecule in aptamer-based chromatographic strip for rapid visual detection of paraquat residue in agricultural products, Sensor Actuat B-Chem 368 (2022) 132237.
[28] L. Wang, S.A. Haruna, W. Ahmad, J. Wu, Q. Chen, Q. Ouyang, Tunable multiplexed fluorescence biosensing platform for simultaneous and selective detection of paraquat and carbendazim pesticides, Food Chem. 388 (2022) 132950.
[29] W.Y. Guo, Y.X. Fu, S.Y. Liu, L.C. Mei, Y. Sun, J. Yin, W.C. Yang, G.F. Yang, Multienzyme-targeted fluorescent probe as a biosensing platform for broad detection of pesticide residues, Anal. Chem. 93 (18) (2021) 7079–7085.
[30] J. Wang, J. Zhang, J. Wang, G. Fang, J. Liu, S. Wang, Fluorescent peptide probes for organophosphorus pesticides detection, J. Hazard Mater. 389 (2020) 122074.
[31] D.A. Jose Nandini, Selective sensing of paraquat by simple off-the-shelf compounds: applications using composite hydrogel beads and smartphone, Sensor Actuat B-Chem 417 (2024) 136070.
[32] S. Che, X. Peng, Y. Zhuge, X. Chen, C. Zhou, H. Fu, Y. She, Fluorescent and colorimetric ionic probe based on fluorescein for the rapid and on-site detection of paraquat in vegetables and the environment, J. Agric. Food Chem. 70 (49) (2022) 15390–15400.
[33] M. Luo, L. Chen, J. Wei, X. Cui, Z. Cheng, T. Wang, I. Chao, Y. Zhao, H. Gao, P. Li, A two-step strategy for simultaneous dual-mode detection of methyl-paraoxon and Ni (II), Ecotoxicol. Environ. Saf. 239 (2022) 113668.
[34] H. Wang, L. Yang, S. Chu, B. Liu, Q. Zhang, L. Zou, S. Yu, C. Jiang, Semiquantitative visual detection of lead ions with a smartphone via a colorimetric paper-based analytical device, Anal. Chem. 91 (14) (2019) 9292–9299.
[35] S.S. Wei, H.Y. Zhang, C.Z. Wang, X.Y. Yin, K.X. Hu, M. Liu, C.Z. Jiang, G.Y. Sun, Portable smartphone platform based on a ratio fluorescence probe for situ visual monition of cardiac disease markers in vitro, Chem Eng J 474 (2023) 145614.
[36] H. Deng, X. Shi, F. Wang, H. Peng, A. Liu, X. Xia, W. Chen, Fabrication of water-soluble, green-emitting gold nanoclusters with a 65% photoluminescence quantum yield via host–guest recognition, Chem. Mater. 29 (3) (2017) 1362–1369.
[37] H. Peng, Z. Huang, H. Deng, W. Wu, K. Huang, Z. Li, W. Chen, J. Liu, Dual enhancement of gold nanocluster electrochemiluminescence: electrocatalytic excitation and aggregation-induced emission, Angew Chem. Int. Ed. Engl. 59 (25) (2020) 9982–9985.
[38] J. Xie, Y. Zheng, J.Y. Ying, Protein-directed synthesis of highly fluorescent gold nanoclusters, J. Am. Chem. Soc. 131 (3) (2009) 888–889.
[39] J.M. Dixon, S. Egusa, Conformational change-induced fluorescence of bovine serum albumin-gold complexes, J. Am. Chem. Soc. 140 (6) (2018) 2265–2271.
[40] M. Luo, J.C. Wei, Y.Y. Zhao, Y.Z. Sun, H.X. Liang, S.P. Wang, P. Li, Fluorescent and visual detection of methyl-paraoxon by using boron-and nitrogen-doped carbon dots, Microchem. J. 154 (2020) 104547.
[41] S. Bhunia, K. Gangopadhyay, A. Ghosh, S.K. Seth, R. Das, P. Purkayastha, Arginine-Modified fluorescent gold nanoclusters for forster resonance energy transfer with a hemicyanine dye: a biofriendly approach, ACS Appl. Nano Mater. 4 (1) (2021) 305–312.
[42] Z. Cheng, L. Gu, Y. Zhao, L. Yang, L. Chen, T. Wang, M. Luo, J. Wei, P. Li, Copper ions assisted fluorescent detection of some dithiocarbamates based on nickel nanocluster with aggregation-induced emission enhancement behavior, J. Hazard Mater. 424 (Pt B) (2022) 127555.
[43] W. Gao, Q. Li, W. Zhong, X. Zhou, Y. Ge, Q.-L. Yan, L. Shang, Gold nanoclusters-engineered dual-emitting nanofibrous film for fluorescent discrimination and visual sensing of explosives, Chem Eng J 456 (2023) 140982.
[44] H.X. Ren, M.X. Mao, M. Li, C.Z. Zhang, C.F. Peng, J.G. Xu, X.L. Wei, A fluorescent detection for paraquat based on beta-CDs-enhanced fluorescent gold nanoclusters, Foods 10 (6) (2021) 1178.

[45] F. Peng, X. Ai, J. Sun, X. Ge, M. Li, P. Xi, B. Gao, Fluorescence lifetime super-resolution imaging unveil the dynamic relationship between mitochondrial membrane potential and cristae structure using the forster resonance energy transfer strategy, Anal. Chem. 96 (27) (2024) 11052–11060.
[46] Y.S. He, C.G. Pan, H.X. Cao, M.Z. Yue, L. Wang, G.X. Liang, Highly sensitive and selective dual-emission ratiometric fluorescence detection of dopamine based on carbon dots-gold nanoclusters hybrid, Sensor Actuat B-Chem 265 (2018) 371–377.
[47] X. Yang, J. Wang, D. Su, Q. Xia, F. Chai, C. Wang, F. Qu, Fluorescent detection of TNT and 4-nitrophenol by BSA Au nanoclusters, Dalton Trans. 43 (26) (2014) 10057–10063.
[48] R.S. Aparna, J.S.A. Devi, P. Sachidanandan, S. George, Polyethylene imine capped copper nanoclusters-fluorescent and colorimetric onsite sensor for the trace level detection of TNT, Sensor Actuat B-Chem 254 (2018) 811–819.
[49] M. Thompson, S.L.R. Ellison, R. Wood, Harmonized guidelines for single-laboratory validation of methods of analysis - (IUPAC technical report), Pure Appl. Chem. 74 (5) (2002) 835–855.
[50] K. Huang, Q. Fang, W. Sun, S. He, Q. Yao, J. Xie, W. Chen, H. Deng, Cucurbit[n]uril supramolecular assemblies-regulated charge transfer for luminescence switching of gold nanoclusters, J. Phys. Chem. Lett. 13 (1) (2022) 419–426.
[51] K.Y. Huang, W.H. Weng, X. Huang, H.X. Huang, H.A.A. Noreldeen, H.H. Deng, W. Chen, Gold nanocluster-based fluorometric banoxantrone assay enabled by photoinduced electron transfer, Nanomaterials 12 (11) (2022) 1861.
[52] K.Y. Huang, X. Huang, X.Y. Fang, S. Cheng, W.M. Sun, H.A.A. Noreldeen, Q. Zhang, H.H. Deng, W. Chen, De novo design of a photoluminescent sensor for baicalin detection via regulating molecule-like charge transfer of gold nanocluster, Sensor Actuat B-Chem 368 (2022) 132197.